

An Open-Source RRAM Compiler

Dimitris Antoniadis*, Andrea Mifsud^{*†}, Peilong Feng^{*†}, Timothy G. Constandinou^{*†‡}

^{*}Department of Electrical and Electronic Engineering, Imperial College London, SW7 2BT, UK

[†]Centre for Bio-Inspired Technology, Institute of Biomedical Engineering, Imperial College London, SW7 2AZ, UK

[‡]Care Research & Technology Centre, UK Dementia Research Institute, UK

{dimitris.antoniadis20, a.mifsud, peilong.feng14, t.constandinou}@imperial.ac.uk

Abstract—Memory compilers are necessary tools to boost the design procedure of digital circuits. However, only a few are available to academia. Resistive Random Access Memory (RRAM) is characterised by high density, high speed, non volatility and is a potential candidate of future digital memories. To the best of the authors’ knowledge, this paper presents the first open source RRAM compiler for automatic memory generation including its peripheral circuits, verification and timing characterisation. The RRAM compiler is written with Cadence SKILL programming language and is integrated in Cadence environment. The layout verification procedure takes place in Siemens Mentor Calibre tool. The technology used by the compiler is TSMC 180nm. This paper analyses the novel results of a plethora of $M \times N$ RRAMs generated by the compiler, up to $M = 128$, $N = 64$ and word size $B = 16$ bits, for clock frequency equal to 12.5MHz. Finally, the compiler achieves density of up to 0.024 Mb/mm^2 .

I. INTRODUCTION

The progress of the technology has lead to an aggressive scaling trend of Integrated Circuits (IC), generating great demand for high density, high speed and low power memories [1]. However, customised memory design is a resource-intensive task [2]–[4]. Therefore, a number of memory compilers has been presented before [2]–[7]. These compilers mainly focus on two types of memories, the volatile memories (e.g. static or dynamic random access memory) and the non volatile memories (e.g. flash memory) [8], [9]. Volatile memories suffer of high power consumption and loss of data on power off, while non volatile memories require high write voltage and suffer of low endurance and low speed [9], [10].

A novel emerging non volatile memory which is characterised by scalability, high speed, high density and low power is the Resistive Random Access Memory (RRAM). RRAM uses memristors in its memory cells [8]–[14]. Therefore, a RRAM compiler is an essential tool to boost the RRAM design procedure and facilitate the research of the memristive device properties [15].

The work presented in [15] described a novel RRAM architecture and demonstrated the results only of the RRAM array generation and its layout verification. This paper extends this work by improving the RRAM architecture described in [15] and presents the first open source RRAM compiler which automatically generates the RRAM including its peripheral circuits, verifies their layout and performs timing characterisation. The features of the RRAM compiler presented in this work are presented in Tab. I. It is clear that the work presented in [15] includes partially only two features of the RRAM compiler presented in this paper. The proposed RRAM compiler includes new features regarding Place and Route (P&R) of memory blocks, co-integration of analogue and digital blocks, layout verification of the whole RRAM

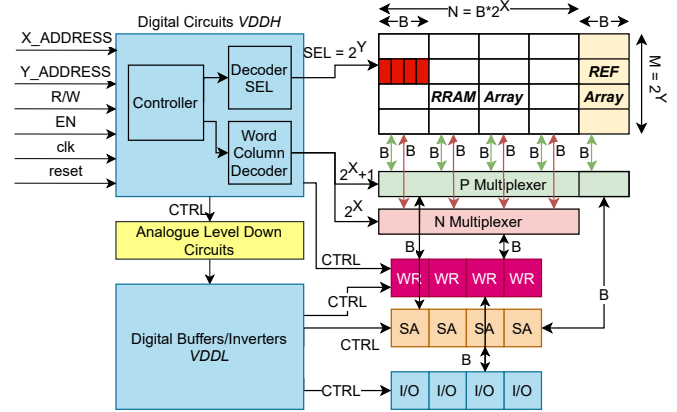


Fig. 1. Simplified block diagram of the RRAM architecture. The size of the RRAM array is $M \times N$, where $M = 2^Y$ and $N = B \cdot 2^X$. Parameter M is the number of rows and parameter N is the number of columns. Parameter B is the length of the memory words. Figure adapted from Fig. 1. in Ref. [15].

TABLE I
OPEN-SOURCE RRAM COMPILERS COMPARISON BETWEEN THIS WORK AND WORK PRESENTED IN [15].

Architecture	Functionalities	Work [15]	This Work
RRAM array	RRAM array generation	Yes	Yes
	Reference cells generation	No	Yes
	Multiplexers generation	No	Yes
	Write Amplifiers generation	No	Yes
Peripheral analogue circuits	Analogue P&R	No	Yes
	Analogue co-integration	No	Yes
	Synthesis	No	Yes
Peripheral digital circuits	Implementation	No	Yes
	Design constraints generation	No	Yes
	GDS and Verilog import	No	Yes
	Mixed-signal P&R	No	Yes
System-level	Mixed-signal co-integration	No	Yes
	Layout generation	No	Yes
	Layout verification	Yes	Yes
	System characterisation	No	Yes

and timing characterisation. The source code of the proposed RRAM compiler has been published on Github:

https://github.com/akdimitri/RRAM_COMPILER

This Section briefly described the background regarding RRAMs, memory compilers and the new features of the proposed RRAM compiler. Section II presents the RRAM architecture and its most important blocks. In Section III the RRAM compiler structure and the characterisation procedure are described. Section IV analyses the results produced by a number of automatically generated designs. Finally, Section V summarises this paper.

II. RRAM ARCHITECTURE

A. RRAM Architecture Overview

A simplified block diagram of the proposed RRAM architecture is shown in Fig. 1. The size of the RRAM array is

$M \times N$, where $M = 2^Y$ and $N = B2^X$. A word of B memory cells is shown under red colour. Blue blocks represent digital circuits, while the rest of them represent analogue circuits. Compared to the architecture presented in [15], reference cells array, B additional of P multiplexer switches and level-shifters between digital blocks have been introduced.

A multiplexer switch consists of a grounding NMOS and a transmission gate. The P multiplexer has one more block of B switches compared to the N multiplexer due to the fact that it connects the reference cells array to the sense amplifiers.

Six signals are needed to control the RRAM in contrast with [15], where only the three very basic were introduced. These are the $X_ADDRESS[X:1]$ signal (address of the desired word column), the $Y_ADDRESS[Y:1]$ signal (address of the desired row), the EN signal (enable chip), the R/W signal (read or write operation), the clock of the chip and the reset signal. The desired word to be read or written is interfaced through I/O ports. A simplified Finite State Machine (FSM) of the digital controller is depicted in Fig. 4.

RRAM uses three power supplies. Memory cells have been designed with high voltage ($VDDH$) technology transistors. Therefore, a number of digital circuits, P and N multiplexer also operate under $VDDH$ voltage. On the other hand sense amplifiers, have to ensure that the voltage applied on the bitlines does not alter the state of the memristor of the memory cells, thus $VDDL$ has been chosen for the sense amplifiers [15]. The sense amplifier incorporates low voltage ($VDDL$) technology transistors. The digital signals that control (CTRL) $VDDL$ circuits have to be levelled down through an analogue level-shifter circuit and they are propagated to the sense amplifiers array and I/O ports through digital buffers or inverters. In order to provide flexibility on the write voltage, a third power supply $VDDW$ has also been included in the design.

The reference cell consists of a NMOS transistor. The drain source resistance of the transistor represents the reference resistance R_{REF} . Its resistance is compared against the corresponding memory cell resistance, when it is sensed by the corresponding sense amplifier. The reference cells are integrated alongside the RRAM array, as they share same lines and have same layout size. The size of the reference cells array is $M \times B$.

B. Write Circuit

The write voltage ($VDDW$) differs based on the memristor materials. The write circuit is shown in Fig. 2. The devices in Figures with thick line make use of transistor models able to support up to $VDDH$ voltage, while the others are able to support up to $VDDL$ respectively. WR_IN can be 0 V or $VDDL$. Transistors $MN1$, $MN2$, $MP1$, $MP2$ and $INV2$ form a conventional level-shifter with positive feedback [16]. Thus, if WR_IN is digital 0, which is modelled in this implementation as Low Resistance State (LRS), then Q will go high, as such, P will be $VDDW$ and N will be 0 V. On the contrary, if WR_IN is digital 1 or $VDDL$, which is modelled in this implementation as High Resistance State (HRS), then P will be 0 V and N will be $VDDW$. These values will be propagated to the desired memory cell through the P and N multiplexers.

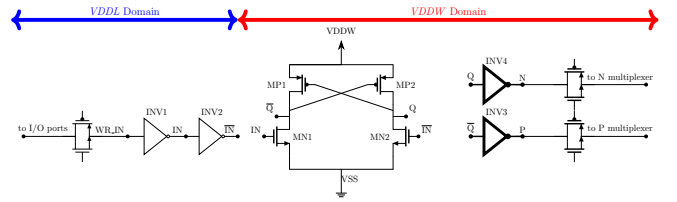


Fig. 2. Write circuit. The input signal at I/O port is a value of 0 or $VDDL$, thus this value has to be levelled up to $VDDW$ and then to be propagated correctly to the corresponding P and N lines.

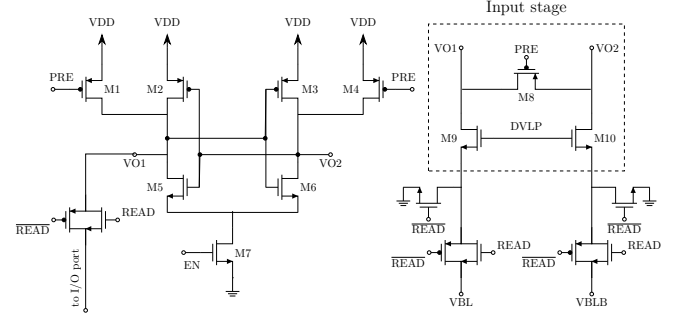


Fig. 3. Sense amplifier circuit. On the left side, a typical cross coupled sense amplifier is shown. The input stage is located on the right. Low impedance of NMOS transistor is used to achieve fast read operation and avoid large loading time duration on bitlines.

C. Sense Amplifier

The sense amplifier is based on those presented in [17], [18] and it is shown in Fig. 3. Transistors $M2$, $M5$, $M3$, $M6$ form a typical cross coupled inverters sense amplifier. Transistors $M1$ and $M4$ precharge $VO1$, $VO2$ to VDD . In this case VDD refers to $VDDL$. A common gate configuration is used for the input stage, keeping the input impedance ($M9$ and $M10$ source terminal) as low as possible. Transistors $M9$ and $M10$ operate in triode region and they force a low voltage on bitlines VBL , $VBLB$. Transistor $M8$ is an equaliser that ensures that equal values are set on $VO1$ and $VO2$. Three additional transistors forming a transmission gate and a grounding NMOS, enable the sense of the memory cell when read operation is executed. Further to this, there is also a transmission gate that connects $VO1$ to I/O ports.

The sense amplifier operates in three phases. Its operation is illustrated in Fig. 6. When $READ$ signal is high, phase 1 starts. Signal PRE remains low, $DVLP$ goes high and current is drawn from the memory cell and the reference cell. In phase 2, PRE goes high, therefore, $VO1$ and $VO2$ are no longer equal and the voltage difference, which is developed between them, is rapidly enhanced. In phase 3, $DVLP$ goes low and EN (or EN_SA) goes high, forcing the result to rail to rail output voltage value. In Fig. 6, vertical lines $READ$ TEST 1 and $READ$ TEST 2 show the moment where EN_SA is set to high and the output of the first ($Z_SA[0]$) and the second ($Z_SA[1]$) sense amplifier has been propagated to the bus ($Z_BUS[3:0]$) of the tri state buffers (I/O ports).

III. RRAM COMPILER

The RRAM compiler is written in SKILL language and is invoked by Command Interpreter Window (CIW) of Cadence Virtuoso 6.1.8 [19], [20]. The very basic arguments are the dimensions (M , N , B) of the memory. Further optional arguments, such as the minimum clock frequency can be specified.

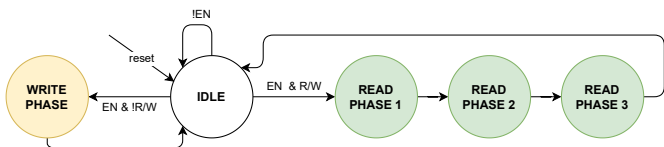


Fig. 4. Simplified finite state machine of the controller of the RRAM with respect to the circuits of Fig. 1. If EN and $\overline{R\overline{W}}$ are received, then the controller generates necessary signals to execute write operation. On the other hand, if EN and RW is received, read operation begins. Read procedure is completed in three phases based on the three-phase operation of the sense amplifier.

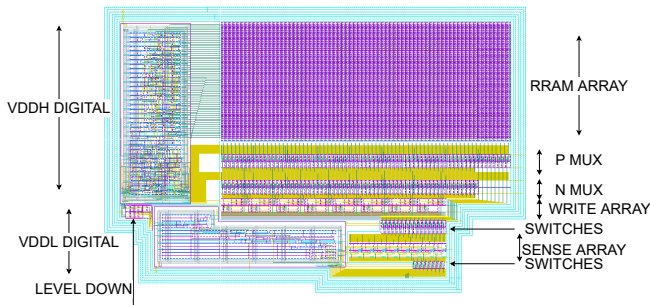


Fig. 5. Generated layout by RRAM compiler. The dimensions of this circuit are $M = 64$, $N = 64$ and $B = 8$. Its size is $524.3 \mu\text{m} \times 353.5 \mu\text{m}$.

The RRAM compiler procedure follows the features presented from top to bottom in Tab. I. The RRAM compiler makes use of Cadence Virtuoso for analogue design and Cadence Genus and Innovus for digital design [21]–[26]. It also verifies the layout correctness of the generated RRAMs by executing Design Rule Checking (DRC) and Layout Versus Schematic (LVS) tests in Mentor Calibre tool [27], [28]. The post-layout view of the RRAM generated by Parasitic Extraction (PEX) tool of Mentor Calibre is used in the timing characterisation procedure. The timing characterisation procedure is invoked by an automatically generated OCEAN script [29]. An example of an automatically generated layout by the RRAM compiler is shown in Fig. 5.

The RRAM characterisation procedure generates a testbench which includes the RRAM block and a verilog block with test signals. The post-layout view of the analogue part of the RRAM and the P&R verilog netlist of the digital circuits are used by the mixed signal simulator in Cadence Virtuoso. The automatically generated RRAMs are tested for Typical Typical (TT), Fast Slow (FS), Slow Fast (SF), Slow Slow (SS) and Fast Fast (FF) NMOS and PMOS models at nominal corner. During the simulation, the Standard Delay Format (SDF) files produced by Innovus after P&R are used to provide realistic results for the digital circuits. The testbench performs initially a reset and then two extreme conditions write (W1, W2) and two read (R1, R2) tests.

By inspection of Fig. 5, it is clear that the worst case read/write operation occurs for the words that are located at the top right corner of the layout, where is the furthest distance from the read/write circuits. Therefore, the loading time of the lines involved in read/write operation for these cells will be the greatest. In the first write test (W1), the word is located at position $X_ADDRESS = 2^X - 1$ and $Y_ADDRESS = 2^Y$. This word is the second to the last word on the top row of the RRAM array. The LRS and HRS values depend on the material characteristics. It is well known that a number of

memristors get resistance values in the range of a few Ohms to tens of kOhms [14], [30]. Given that, the memristance of the memory cells is emulated with a resistance equal to $1 \text{ M}\Omega$ as an extreme value to examine worst case settling time across the memory cell. The desired value to be written on this test is $10\dots10$, resulting in V_{PN} (Voltage across P and N terminal of memory cell) being positive for a 0, and negative for a 1. The voltage across P and N terminals of the word is checked at $0.4 \times \text{clock time}$ later than the write phase has started by the controller. This is because the clock waveform that is used by the synthesis has 50% duty cycle. Therefore, this value has to be set up in time. The test checks whether, at this point of time, the desired V_{PN} is greater than $0.7 \times VDDW$ when $I/O = 0$ or V_{PN} is less than $-0.7 \times VDDW$ when $I/O = 1$. As a default value, $VDDW$ is set by the compiler to 3.3 V . Memristors write voltage can vary from around 2 V to up to 10 V or more [14]. The limit $0.7 \times VDDW$ is a demonstration limit and should be set according to the device characteristics. The W2 test performs the same checks. The only difference is that the desired value to be written is the complementary one $01\dots01$ compared to the previous test.

Similarly, two tests are executed to verify correctness of the read operation. In read tests, the last word of the top row is selected. The address of this word is $X_ADDRESS = 2^X$ and $Y_ADDRESS = 2^Y$. In this case, the memristance of each memory cell is also emulated with a resistor (representing extreme HRS and LRS values). In the first read (R1) test, the resistances of the cells of the word under test are initialised with respect to a value $a < 1$. By default a is set equal to 0.3. Then, LRS is equal to $a \cdot R_{REF}$ and HRS is equal to $a^{-1} \cdot R_{REF}$. In this case, R_{REF} was set equal to $32.5 \text{ k}\Omega$ as a typical median resistance value of a memristor. In the first read test (R1), the word is initialised to value LRS, HRS...LRS, HRS. Therefore, for HRS, logical 1 should be read at the output 1 and for LRS, logical 0 respectively. Same as previously, the check takes place $0.4 \times \text{clock time}$ later than the third phase of the read procedure, as the read value has to be set up in time for the tri state buffers to hold it. In this case, regarding the cells that have been initialised with the HRS value, it is checked whether the value at the output of the sense amplifier is greater than $0.83 \times VDDL$. For those which have been initialised with the LRS value, it is checked if the value at the output of the sense amplifier is less than $0.16 \times VDDL$. The second read test is the same as above. The only difference is that the complementary value HRS, LRS...HRS, LRS is set on the word under test. An example of the R1, R2 tests for the first two bits of the word under test in the memory is shown in Fig. 6.

IV. RESULTS

Multiple sizes were tested, as it is shown on Tab. II. Maximum clock frequency was set to 25 MHz , as this is the maximum clock frequency that meets the digital synthesis design constraints. A table with the results for 12.5 MHz is shown on Tab. II. Memories succeed in all write tests, while some of them fail to pass the read tests mainly for FS and FF corners. This occurs due to the fact that only one output of the sense amplifiers is used in this topology. This output is connected to a bus while the other one is floating, as such,

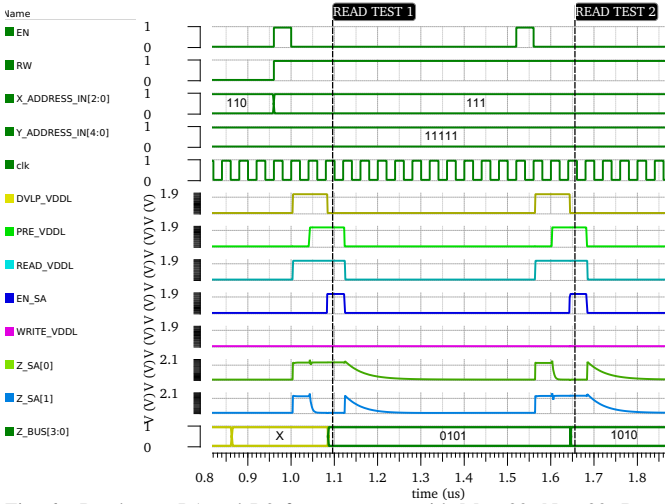


Fig. 6. Read tests R1 and R2 for a memory with $M = 32$, $N = 32$, $B = 4$ and clock period equal to 40 ns. It should be noted that the signals shown here start counting by zero (0). The vertical lines, show the moment when checks are performed. The addresses of the word under test will be in this case $X_ADDRESS = 2^X - 1 = 2^3 - 1 = {}_{(10)}7 = {}_{(2)}111$ and $Y_ADDRESS = 2^Y - 1 = 2^5 - 1 = {}_{(10)}31 = {}_{(2)}11111$. Signals Z_SA are the VO1 signals with respect to Fig. 3 of the corresponding sense amplifiers. Signal Z_BUS is output of the Tri State Buffer of the RRAM memory. The rest of the signals are the digital control signals that have been levelled down.

there is an imbalance between the driving output load. The author suggests that the sense amplifiers should be isolated by connecting their input/output to buffers. Write operations are correct (all corners) for an up to 8 kb memory and write time 80 ns. Write test, in greater frequencies, may fail due to the big loading time on the terminals of the memory cells. Additionally, read operations are correct (all corners) for an up to 8 kbit memory with $B = 4$ and access time approximately equal to $2/3$ clock, which is 160 ns. Fastest access time is equal to 80 ns and it is achieved for an up to 1 kbit memory with $B = 4$ and clock frequency 25 MHz. The best density (RRAM bit size / RRAM layout size) achieved by the compiler is 0.024 Mb/mm^2 in TSMC 180 nm technology.

Furthermore, by using three power supplies the design becomes less robust and complex. The author suggests that the architecture could be redesigned and simplified by using only one power supply $VDDH$. The write circuit could be replaced with a programmable digital to analogue converter (DAC) to provide the necessary flexibility on the write voltage. Finally, the reference array could be potentially replaced by a programmable current mirror.

Memristance is a property that arises particularly in thin film devices, which are extremely small in size. The current implementation takes into account their size by placing corresponding pins on the top metals of RRAM cells. In this way, memristors can be placed on top of the RRAM array after the CMOS fabrication of the memory. However, the RRAM compiler uses ideal resistors for their emulation in the timing characterisation procedure. As a future improvement, the authors suggest the use of a realistic model of a memristor in order to account for even more realistic results. Additionally, temperature variation should be included in the tests. Furthermore, the power estimation of the RRAM should be introduced in future versions of the RRAM compiler.

A direct comparison between RRAMs cannot be made

TABLE II
RESULTS PRODUCED BY MEMORY CHARACTERISATION PROCEDURE WITH CLOCK 80 NS (12.5 MHz).

N	M	B	Nominal	FS	SF	SS	FF	report
32	32	4	pass	pass	pass	pass	pass	link
64	16	4	pass	pass	pass	pass	pass	link
64	16	8	fail (R1)	fail (R1, R2)	pass	pass	fail (R1, R2)	link
64	32	4	pass	pass	pass	pass	pass	link
64	32	8	fail (R1, R2)	fail (R1, R2)	pass	pass	fail (R1, R2)	link
64	64	4	pass	pass	pass	pass	pass	link
64	64	8	pass	fail (R1, R2)	pass	near	fail (R1, R2)	link
128	16	4	pass	pass	pass	pass	pass	link
128	16	8	pass	fail (R1, R2)	pass	pass	fail (R1, R2)	link
128	16	16	fail (R1, R2)	link				
128	32	4	pass	pass	pass	pass	pass	link
128	32	8	pass	fail (R1, R2)	pass	pass	fail (R1, R2)	link
128	32	16	fail (R1, R2)	link				
128	64	4	pass	pass	pass	pass	pass	link
128	64	8	pass	fail (R1, R2)	pass	pass	fail (R1, R2)	link
128	64	16	fail (R1, R2)	link				

TABLE III
MEMORIES DENSITY COMPARISON.

Ref.	Feature Size	Technology	Mb/mm ²
[31]	40 nm	CMOS	0.94
[32]	45 nm	CMOS	0.33
[3]	45 nm	FreePDK45	0.826
[33]	65 nm	CMOS	0.77
[34] ¹	65 nm	CMOS/memristor	0.54
This work ²	180 nm	CMOS/memristor	0.024
[15] ³	180 nm	CMOS/memristor	0.082
[35] ³	180 nm	CMOS	0.067
[3]	0.5 μm	SCMOS	0.005

¹ RRAM subarray chip. ² Memory chip density. ³ Memory cell size.

as they refer to different sizes and different materials. A density comparison between volatile memories, this work and the RRAM sub-arrays generated by the corresponding RRAM compilers presented in [34] and [15] is shown on Tab. III. RRAM compilers generate quite dense designs similar to SRAM designs. This work achieves approximately same density with an SRAM designed at TSMC 180 nm technology. The memory cell of the proposed implementation is relatively big to ensure robustness and low mismatch. It can be further reduced to improve the density. The optimal size of the RRAM cell should be further investigated. Fully custom made RRAMs exploiting multi state bit memory cells can achieve up to 6.66 Mb/mm^2 and read/write access time less than 200 ns for up to 4 Mb designs [36]–[38]. The RRAM compiler presented in [39] exploits 3D IC design to further improve density, however the results are normalised and a direct comparison cannot be made.

V. CONCLUSION

Taking everything into consideration, this paper presented the first open source RRAM compiler which automatically generates the RRAM array, the peripheral circuits and provides layout verification and timing characterisation. In this way, a number of memristors can be integrated and tested by using the automatically generated designs. Finally, the RRAM compiler serves as a great tool for both industry and academia in order to boost the RRAM design procedures and the investigation of the RRAM properties.

ACKNOWLEDGMENT

The authors acknowledge the support of the EPSRC FORTE Programme Grant (EP/R024642/1).

REFERENCES

- [1] Y. Chen, "ReRAM: History, status, and future," *IEEE Transactions on Electron Devices*, vol. 67, no. 4, pp. 1420–1433, 2020, [Online].
- [2] Y. Xu *et al.*, "A flexible embedded SRAM IP compiler," in *2007 IEEE ISCAS*. IEEE, 2007, pp. 3756–3759, [Online].
- [3] M. R. Guthaus *et al.*, "Openram: An open-source memory compiler," in *2016 IEEE/ACM ICCAD*. IEEE, 2016, pp. 1–6, [Online].
- [4] T. Shah *et al.*, "FabMem: A multiported RAM and CAM compiler for superscalar design space exploration," 2010, [Online].
- [5] S. Wu *et al.*, "A 65nm embedded low power SRAM compiler," in *13th IEEE Symposium on DDECS*. IEEE, 2010, pp. 123–124, [Online].
- [6] R. Goldman *et al.*, "Synopsys' educational generic memory compiler," in *10th EWME*. IEEE, 2014, pp. 89–92, [Online].
- [7] M. Clinton *et al.*, "A 5GHz 7nm L1 cache memory compiler for high-speed computing and mobile applications," in *2018 IEEE ISSCC*. IEEE, 2018, pp. 200–201, [Online].
- [8] A. Chen, "A review of emerging non-volatile memory (NVM) technologies and applications," *Solid-State Electronics*, vol. 125, pp. 25–38, 2016, [Online].
- [9] F. Zahoor *et al.*, "Resistive random access memory (RRAM): an overview of materials, switching mechanism, performance, multilevel cell (MLC) storage, modeling, and applications," *Nanoscale research letters*, vol. 15, no. 1, pp. 1–26, 2020, [Online].
- [10] S. Maheshwari *et al.*, "Hybrid CMOS/memristor circuit design methodology," *arXiv preprint arXiv:2012.02267*, 2021, [Online].
- [11] D. B. Strukov *et al.*, "The missing memristor found," *nature*, vol. 453, no. 7191, pp. 80–83, 2008, [Online].
- [12] J. J. Yang *et al.*, "Memristive devices for computing," *Nature nanotechnology*, vol. 8, no. 1, pp. 13–24, 2013, [Online].
- [13] D. Ielmini *et al.*, "In-memory computing with resistive switching devices," *Nature Electronics*, vol. 1, no. 6, pp. 333–343, 2018, [Online].
- [14] S. Stathopoulos *et al.*, "An electrical characterisation methodology for benchmarking memristive device technologies," *Scientific reports*, vol. 9, no. 1, pp. 1–10, 2019, [Online].
- [15] D. Antoniadis *et al.*, "Open-source memory compiler for automatic RRAM generation and verification," in *2021 IEEE MWSCAS*, 2021, pp. 97–100, [Online].
- [16] D. Dwivedi *et al.*, "Voltage up level shifter with improved performance and reduced power," in *2012 25th IEEE Canadian Conference on Electrical and Computer Engineering (CCECE)*, 2012, pp. 1–4, [Online].
- [17] I. P. Tolić *et al.*, "Design of sense amplifiers for non-volatile memory," in *2019 42nd International Convention on Information and Communication Technology, Electronics and Microelectronics (MIPRO)*. IEEE, 2019, pp. 59–64, [Online].
- [18] M. Suma *et al.*, "Analysis of sense amplifier circuits in nanometer technologies," in *2017 Fourth International Conference on Signal Processing, Communication and Networking (ICSCN)*. IEEE, 2017, pp. 1–4, [Online].
- [19] Cadence *SKILL Language Reference Product Version ICADVM20.1*, Cadence Design Systems, San Jose, USA, 2021.
- [20] Cadence *SKILL Language User Guide Product Version ICADVM20.1*, Cadence Design Systems, San Jose, USA, 2021.
- [21] *Virtuoso Analog Design Environment XL User Guide Product Version IC6.1.8*, Cadence Design Systems, San Jose, USA, 2021.
- [22] *Virtuoso Layout Suite XL User Guide Product Version IC6.1.8*, Cadence Design Systems, San Jose, USA, 2021.
- [23] *Virtuoso Schematic Editor User Guide Product Version ICADVM20.1*, Cadence Design Systems, San Jose, USA, 2021.
- [24] *Virtuoso ADE Explorer User Guide Product Version ICADVM20.1*, Cadence Design Systems, San Jose, USA, 2021.
- [25] *Genus User Guide 20.1 Product Version 20.1*, Cadence Design Systems, San Jose, USA, 2020.
- [26] *Innovus User Guide Product Version 21.10*, Cadence Design Systems, San Jose, USA, 2021.
- [27] *Calibre® Interactive™ (New GUI) User's Manual*, Siemens Mentor, 2020.
- [28] *Calibre® Verification User's Manual*, Siemens Mentor, 2020.
- [29] *OCEAN Reference Product Version ICADVM20.1*, Cadence Design Systems, San Jose, USA, 2021.
- [30] K. Nikiruy *et al.*, "A precise algorithm of memristor switching to a state with preset resistance," *Technical Physics Letters*, vol. 44, no. 5, pp. 416–419, 2018, [Online].
- [31] S. Miyano *et al.*, "Highly energy-efficient SRAM with hierarchical bit line charge-sharing method using non-selected bit line charges," *IEEE JSSC*, vol. 48, no. 4, pp. 924–931, 2013, [Online].
- [32] S. O. Toh *et al.*, "Characterization of dynamic SRAM stability in 45 nm CMOS," *IEEE JSSC*, vol. 46, no. 11, pp. 2702–2712, 2011, [Online].
- [33] K. Kushida *et al.*, "A 0.7 V single-supply SRAM with 0.495 μm^2 cell in 65 nm technology utilizing self-write-back sense amplifier and cascaded bit line scheme," *IEEE JSSC*, vol. 44, no. 4, pp. 1192–1198, 2009, [Online].
- [34] E. Lee *et al.*, "A ReRAM memory compiler with layout-precise performance evaluation," in *2019 IEEE SOI-3D-Subthreshold Microelectronics Technology Unified Conference (S3S)*. IEEE, 2019, pp. 1–3, [Online].
- [35] C. A. Kumar *et al.*, "Performance analysis of low power 6T SRAM cell in 180nm and 90nm," in *2016 2nd International Conference on AEEICB*, 2016, pp. 351–357, [Online].
- [36] S.-S. Sheu *et al.*, "A 4Mb embedded SLC resistive-RAM macro with 7.2ns read-write random-access time and 160ns MLC-access capability," in *2011 IEEE International Solid-State Circuits Conference*, 2011, pp. 200–202, [Online].
- [37] S.-S. Sheu *et al.*, "Fast-write Resistive RAM (RRAM) for embedded applications," *IEEE Design Test of Computers*, vol. 28, no. 1, pp. 64–71, 2011, [Online].
- [38] M. Zangeneh *et al.*, "Design and optimization of nonvolatile multibit 1T1R Resistive RAM," *IEEE Transactions on Very Large Scale Integration (VLSI) Systems*, vol. 22, no. 8, pp. 1815–1828, 2014, [Online].
- [39] E. Lee *et al.*, "A ReRAM memory compiler for monolithic 3D integrated circuits in a carbon nanotube process," *ACM Journal on Emerging Technologies in Computing Systems (JETC)*, vol. 18, no. 1, pp. 1–20, 2021, [Online].